Earth and Planetary Science Letters 403 (2014) 380–392

Contents lists available at ScienceDirect

Earth and Planetary Science Letters

www.elsevier.com/locate/epsl

The P-wave boundary of the Large-Low Shear Velocity Province beneath the Pacific

Daniel A. Frost *, Sebastian Rost

University of Leeds, School of Earth and Environment, Leeds, West Yorkshire, United Kingdom

ARTICLE INFO

Article history:
Received 29 March 2014
Received in revised form 21 June 2014
Accepted 24 June 2014
Available online 31 July 2014
Editor: P. Shearer

Keywords:
P-waves
LLSVP
deep earth seismology
lower mantle
seismic body-waves
USArray

ABSTRACT

The Large Low Shear Velocity Provinces (LLSVPs) in the lower mantle represent volumetrically significant thermal or chemical or thermo-chemical heterogeneities. Their structure and boundaries have been widely studied, mainly using S-waves, but much less is known about their signature in the P-wavefield. We use an extensive dataset recorded at USArray to create, for the first time, a high-resolution map of the location, shape, sharpness, and extent of the boundary of the Pacific LLSVP using $P(P_{diff})$-waves. We find that the northern edge of the Pacific LLSVP is shallow dipping (26° relative to the horizontal) and diffuse (~120 km wide transition zone) whereas the eastern edge is steeper dipping (70°) and apparently sharp (~40 km wide). We trace the LLSVP boundary up to ~500 km above the CMB in most areas, and 700 km between 120° and 90°W at the eastern extent of the boundary. Apparent P-wave velocity drops are ~1–3% relative to PREM, indicating a strong influence of LLSVPs on P-wave velocity, at least in the high-frequency wavefield, in contrast to previous studies. A localised patch with a greater velocity drop of ~15–25% is detected, defined by large magnitude gradients of the travel-time residuals. We identify this as a likely location of an Ultra-Low Velocity Zone (ULVZ), matching the location of a previously detected ULVZ in this area. The boundary of a separate low velocity anomaly, of a similar height to the LLSVP, is detected in the north–west Pacific, matching tomographic images. This outlier appears to be connected to the main LLSVP through a narrow channel close to the CMB and may be in the process of joining or splitting from the main LLSVP. We also see strong velocity increases in the lower mantle to the east of the LLSVP, likely detecting subducted material beneath central America. The LLSVP P-wave boundary is similar to that determined in high-resolution S-wave studies and follows the −0.4% ΔV_S iso-velocity contour in the S40RTS tomography model. Additionally, the LLSVP boundary roughly matches the shape of the −0.4% ΔV_P iso-velocity contour of the P-wave model GyPSuM but defines an area more similar to that defined by the 0.0% V_P iso-velocity contour. High resolution P-wave velocity determination allows for estimation of the ratio of P- and S-wave velocity anomalies ($R_{S,P}$) which can be used to indicate dominantly thermal or chemical control of seismic velocities. Although the $R_{S,P}$ is found here to be approximately 2.4, which is indicative of a thermo-chemical anomaly. However, this result contains a large amount of uncertainty and the implications for the origin of LLSVPs likely remain inconclusive. Nonetheless, other observations of the Pacific LLSVP are consistent with a thermo-chemical anomaly whose shape and boundary sharpness are controlled by proximity to active and past subduction.

1. Introduction

Tomographic S-wave images of the lowermost mantle are dominated by two nearly antipodal volumes of strongly reduced seismic S-wave velocity (e.g. Dziewonski, 1984; Ritsema et al., 1999; Panning and Romanowicz, 2006; Simmons et al., 2010; Ritsema et al., 2011; Lay and Garnero, 2011). These structures are commonly referred to as Large-Low Shear Velocity Provinces (LLSVP) and are characterised by a shear-wave (S-wave) velocity drop of about 2% in tomography models and 3–5% in high-resolution S-wave studies (Ritsema et al., 1997, 1998; Ni and Helmberger, 2003; Wang and Wen, 2007; Lay and Garnero, 2011) relative to 1D Earth models (e.g. Dziewonski and Anderson, 1981; Kennett and Engdahl, 1991) extending from the Core Mantle Boundary (CMB) to ~1000 km above (Burke et al., 2008; Helmberger et al., 2009). Normal modes and free-air gravity anomalies point to an increased density within the LLSVPs (Ishii and Tromp, 1999). The structure and location of the LLSVPs are very consistent between different tomographic S-wave models (Lekic et al., 2012) but are less well constrained for P-waves. The LLSVPs might have an influence on surface tectonics with hotspot volcanism showing a strong correlation with the edges of the LLSVPs (Williams et al., 1998; Thorne et al., 2004), as do the palaeo-locations of Large Igneous Provinces (LIPS) (Torsvik

* Corresponding author.

http://dx.doi.org/10.1016/j.epsl.2014.06.046

et al., 2006), and geochemical anomalies (Dupre and Allegre, 1983; Hart, 1984; Castillo, 1988). LLSVPs are also suggested to influence the pattern of outer core convection, thereby modifying the generation of the Earth's magnetic field (Gubbins et al., 2007; Davies et al., 2008). Both S- and P-wave tomographic images indicate that the LLSVPs are surrounded by high seismic velocities relative to 1D models which have been related to pooling of subducted slabs, described as "slab graveyards" (Richards and Engebretson, 1992; Garnero and Helmberger, 1995). This is supported by seismic evidence showing the strongest seismic velocity gradients at the edges of these structures (Thorne et al., 2004) and sharp boundaries to the LLSVPs (resolved only with S-waves) (Ritsema et al., 1997, 1998; Ni et al., 2002; Ni and Helmberger, 2003; Wang and Wen, 2004; Helmberger and Ni, 2005; To et al., 2005; Ford et al., 2006; Wang and Wen, 2007; He and Wen, 2012). LLSVPs might be related to smaller-scale lowermost mantle structures such as Ultra-Low Velocity Zones (ULVZs) (Garnero and Helmberger, 1995; Rost and Garnero, 2004; Rost et al., 2005; Lay et al., 2006) and compositional heterogeneities (Hedlin and Shearer, 2000; Frost et al., 2013), through internal mixing and settling of denser material (McNamara et al., 2010). An enigmatic feature of LLSVPs is the apparent anti-correlation between S-wave and bulk-sound speed resolved in global tomographic images (Masters et al., 2000). This combination of geophysical observations has led to a model of the LLSVPs as dense thermo-chemical piles (McNamara and Zhong, 2005), although purely thermal models of LLSVPs have also been discussed (Schuberth et al., 2009; Davies et al., 2012).

Within the mineralogy of mantle materials, the transition from perovskite to post-perovskite under lower mantle pressures is calculated to be sensitive to temperature, primarily occurring in relatively cold conditions, such as regions related to subduction (Murakami et al., 2004; Oganov and Ono, 2004). The sharp velocity increase with depth resulting from the transition to post-perovskite has been discussed as the source of the D″ reflector (Murakami et al., 2004; Oganov and Ono, 2004). The apparent absence of the D″ reflector within LLSVPs implies that LLSVPs are likely hotter than the surrounding mantle, where the D″ reflector is more commonly seen (Thomas et al., 2004; Hutko et al., 2009).

Geodynamic models of dense thermo-chemical piles indicate that the location of LLSVPs can be explained well by material slightly denser than the surrounding mantle. Some models require density and bulk-modulus increases of ∼2 and ∼7%, respectively, to maintain the shape of the anomaly (Tan and Gurnis, 2005, 2007). In other studies, a density increase of 2 to 5% seems sufficient to avoid entrainment of the material in mantle flow (McNamara and Zhong, 2005; Garnero and McNamara, 2008) and allows stable piles over the lifetime of the Earth. In these models the dense material is swept into the approximate location and shapes as seen in the lower mantle from tomographic images if constraints of the recent to present subduction history are taken into account (McNamara and Zhong, 2005). The location of the LLSVPs seems to be a consequence of the orientation of the Earth's rotation axis and the overall dynamics of the Earth's mantle (Richards et al., 1997; Steinberger and Torsvik, 2008; Trønnes, 2010).

The origin of the LLSVPs is widely debated with models that can be roughly divided into those requiring accumulation of primordial material through incomplete segregation of the mantle (Becker et al., 1999; Labrosse et al., 2007), and those where LLSVPs are built up by the segregation of subduction products (i.e. the deposition of mid-oceanic ridge basalts (MORB)) (Christensen and Hofmann, 1994; Brandenburg and van Keken, 2007; van Keken et al., 2010). Segregation of MORB as a source for lower mantle heterogeneities would be a continuous process (Christensen and Hofmann, 1994), while isotope studies require an untapped primordial reservoir that might have been formed as early as 400 to 500 Myr into Earth's history (Boyet and Carlson, 2005; Carlson and Boyet, 2006). Recent combined geodynamical, seismological and mineral physics studies indicate that it might be difficult to fit the geophysical characteristics of LLSVPs by MORB accumulation (Deschamps et al., 2012; Li and McNamara, 2013).

The location of LLSVPs at the CMB is well resolved using S-wave tomographic techniques (Lekic et al., 2012), although resolution of the precise boundaries is poor close to the CMB (Panning and Romanowicz, 2006; Lay and Garnero, 2011), which, instead, can be determined with high-resolution travel-time and waveform studies (To et al., 2005; Ford et al., 2006; He and Wen, 2009, 2012). Nonetheless, the shape of the LLSVPs above the D″ region is less well resolved due to a decay of resolution in tomographic images. Despite wide ranging agreement for S-waves, P-wave tomography models fail to agree on the location of the LLSVPs, and no attempt has been made for a high resolution determination of the boundaries of the Pacific LLSVP using P-wave travel times and waveforms as has been done with S-waves (He and Wen, 2012). Indeed, studies report little to no response to the African LLSVP structure from P-waves in terms of either travel-times or waveforms (Helmberger and Ni, 2005).

The location of the LLSVP boundary and, especially, the steepness of its edges can inform about the viscosity of the LLSVP material and the convective support of the structure (Tan and Gurnis, 2005; McNamara and Zhong, 2005; Tan and Gurnis, 2007). Furthermore, a comparison between P- and S-wave structure will allow better differentiation between thermal and thermo-chemical models of LLSVPs (Robertson and Woodhouse, 1996a, 1996b; Karato, 2003). To this end, we attempt to resolve the detailed location of the Pacific LLSVP (despite working with P-waves we will continue to use the term LLSVP to refer to the thermo-chemical piles). Using the lateral extent of USArray (Meltzer et al., 1999) we are able to map the precise location of the Pacific LLSVP, especially in the north and east of the LLSVP. We use travel-times of lower mantle turning and core-grazing P-waves to determine the LLSVP boundary location. We utilise a wide range of epicentral distances and back azimuths to track the vertical and lateral extent of the LLSVP, respectively. We correct for both upper mantle (down to depths of 1600 km) and crustal structure in the source and receiver regions using the combined P-wave geodynamic tomography model GyPSuM (Simmons et al., 2010) and the crustal structure model Crust1.0 (Laske et al., 2012). We resolve the P-wave boundary of the LLSVP as the transition from positive to negative travel time anomalies. The observed boundary tracks the 0% contour of the P-wave model GyPSuM well, and partially agrees with the S-wave velocity structure.

2. Method

We employ data from USArray, mainly the Transportable Array (TA) with additional permanent "backbone" stations. USArray has an approximate station spacing of 70 km and is deployed on a grid system (Fig. 1). The array has been operational between 2004 and 2014, moving across the USA with stations being relocated roughly every two years. At any one time, there have been between 300 and 600 operating stations. Using this network configuration allows for a wide sampling of the lowermost mantle, both laterally and vertically, due to the large distance and azimuth range covered by the stations.

We search the Reviewed Events Bulletin (REB) catalogue for events with magnitudes of 5.0 and above and select those that have distances from ∼85° to ∼95° from the centre-point of the array. We concentrate on events from the Indonesian Arc, Tonga Trench, south-eastern Pacific, and South-American Trench. The great-circle paths of these events to USArray are best suited

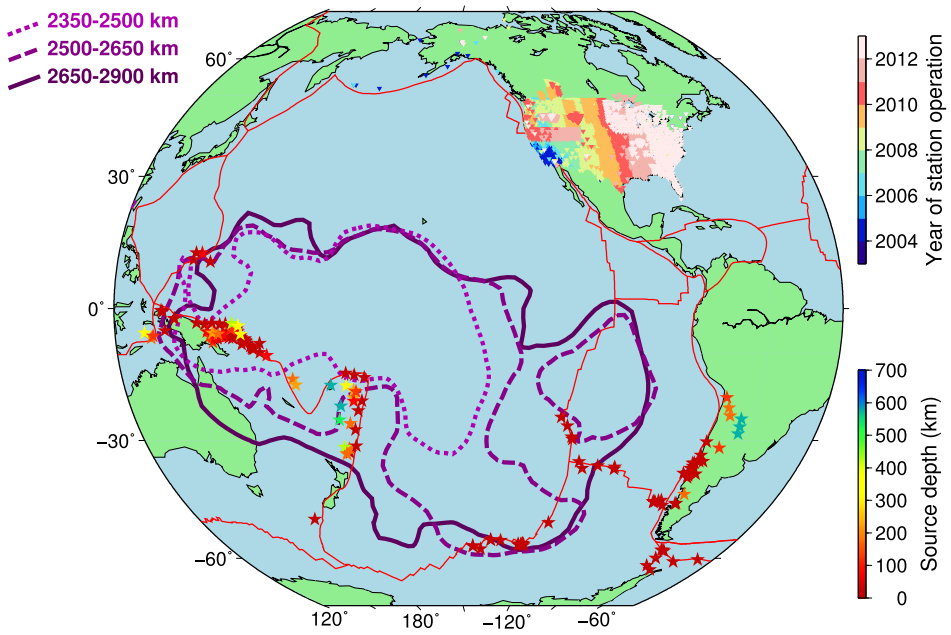

Fig. 1. Events and stations used in this study. Events are denoted as stars with colour indicating source depth. A full listing of earthquakes used is shown in the supplementary material (Supplementary Table 1). Stations are shown as inverted triangles with colour indicating year of deployment. Plate boundaries (red lines) from NUVEL-1 (DeMets et al., 1990) are shown along with the area covered by the Pacific LLSVP, as defined by the -0.4% V_P contour in GyPSuM (Simmons et al., 2010), shown as the purple contours. The LLSVP contours are drawn at 2350–2500 km depth, 2500–2650 km, and 2650–2900 km, as defined by the depth slices in the tomography model.

to sample the northern and eastern edges of the Pacific LLSVP. Although events at any depth, including crustal events, are used in areas with low seismicity, we preferentially use events with depths $\geq$30 km due to their simpler source mechanisms and to reduce travel-time anomalies from crustal and uppermost mantle heterogeneities in the source region. The selected events and stations are shown in Fig. 1.

For each event, data are de-spiked, re-sampled at 40 samples/s, and bandpass filtered. We filter between 0.5 and 1.6 Hz, order 2, as this was found to be best to extract P and P_{diff} arrivals from the noise, where the order controls the rate of decay of energy with frequencies outside of the pass-band. Noisier events, where the P-wave is less clear relative to the noise, are filtered with order 3 or 4, defining a sharper frequency cut-off. To retain as much waveform information as possible, we use the lowest possible order filter that clearly reveals the first arrivals. We only consider traces at distances between 60° and 120° to observe energy turning in the lower mantle. We then visually inspect each trace to decide whether to include it in further processing, based on the P-wave arrival being obvious above the noise.

We apply an adaptive stacking routine (Rawlinson and Kennett, 2004) to find the best alignment of an ensemble of network stations and to determine travel-time deviations from a 1-D Earth model. The adaptive stacking first applies a move-out correction based on distance through PREM (Dziewonski and Anderson, 1981) and iterates to minimise residual travel-times by maximising the amplitude and coherence of a stack of all traces. All travel-time deviations, therefore, are calculated relative to PREM. We correct for crustal structure on both the source and receiver side and topography on the receiver side by applying travel-time corrections as determined by Crust1.0 (Laske et al., 2012), and for upper mantle structure from the underside of the crust down to 1600 km depth (the shallowest turning depth in our collection) by ray-tracing through the P-wave component of GyPSuM (Simmons et al., 2010) (Fig. 2 and Supplementary Fig. 1). The source side correction applied is static and is only used for events shallower than 24 km, the thickness of the crustal layer in PREM. Using the crustal thickness and velocities from PREM would, particularly in oceanic regions, be inappropriate for waves travelling through the lithosphere. The crustal and mantle corrections allow us to attribute the remaining travel-time residual to structure at depths greater than 1600 km. Travel-time residuals are plotted at the lateral location and depth of the turning point of the ray (Fig. 3). The ray-path is longest at the depth where the ray turns and so has the potential to accumulate the most residual time.

The boundary of the LLSVP is defined by obvious travel-time residual trends. We distinguish between cases where the transition can be clearly identified, i.e. where both positive and negative residuals are separated by zero residual, and where a trend towards the transition is observed, i.e. where there are decreasing or increasing travel-time residuals but no change in sign of the residual, the latter boundary being less well constrained. As the boundary location changes with height, we consider each event individually and separate turning points into a series of 100 km thick radial height bins from the CMB upwards. Events with too few turning-points in a height bin to show either the boundary or a trend towards the boundary are discarded.

For each event, we trace the LLSVP boundary in each height bin, determined visually from the residual travel-times, with the extent of the boundary controlled by the ray coverage. For each height bin, we then take the ensemble of boundaries of all events and define a single boundary which visually best fits the individual measurements (Fig. 4). As an additional measure of the LLSVP boundary, we use the magnitude of the gradient of travel-time residuals. We bin data in $0.5 \times 0.5°$ bins and calculate the average residual. In regions where data fill adjacent bins, we calculate the magnitude of the gradient of the travel-time residuals and visually choose a boundary defined by a line of largest magnitude gradient (Fig. 5). Although this method is more robust as it analyses only the pattern of residual travel-times, rather than the absolute value which can be affected by source depth errors, it is only applicable in regions of dense sampling. In comparison, the absolute travel-time residuals can be used to locate the boundary even when sampling is poor, but the location will be less well constrained. In general, in well sampled regions the results of both methods agree well.

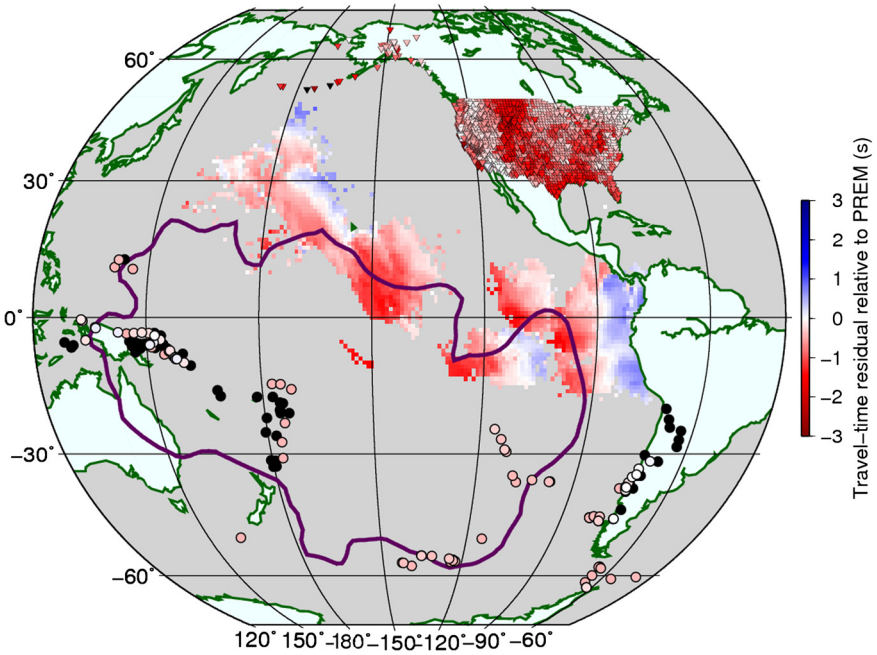

Fig. 2. Crustal and mantle corrections relative to PREM also demonstrating the turning-point coverage of the mantle for all events used. Circles show corrections for crustal structure at the source. Black circles indicate sources deeper than 24 km to which no source-side crustal correction is applied. Triangles show corrections for crustal structure at each station in USArray, averaged over all events which use the station. Background shows corrections for mantle structure along the whole ray-path shown at the turning point of each ray, averaged over all rays turning at that location. Crustal structure is determined from CRUST1.0 (Laske et al., 2012) and mantle structure is determined from the P-wave component of the GyPSuM model (Simmons et al., 2010). The −0.4% V_P contour from GyPSuM is shown by the purple line.

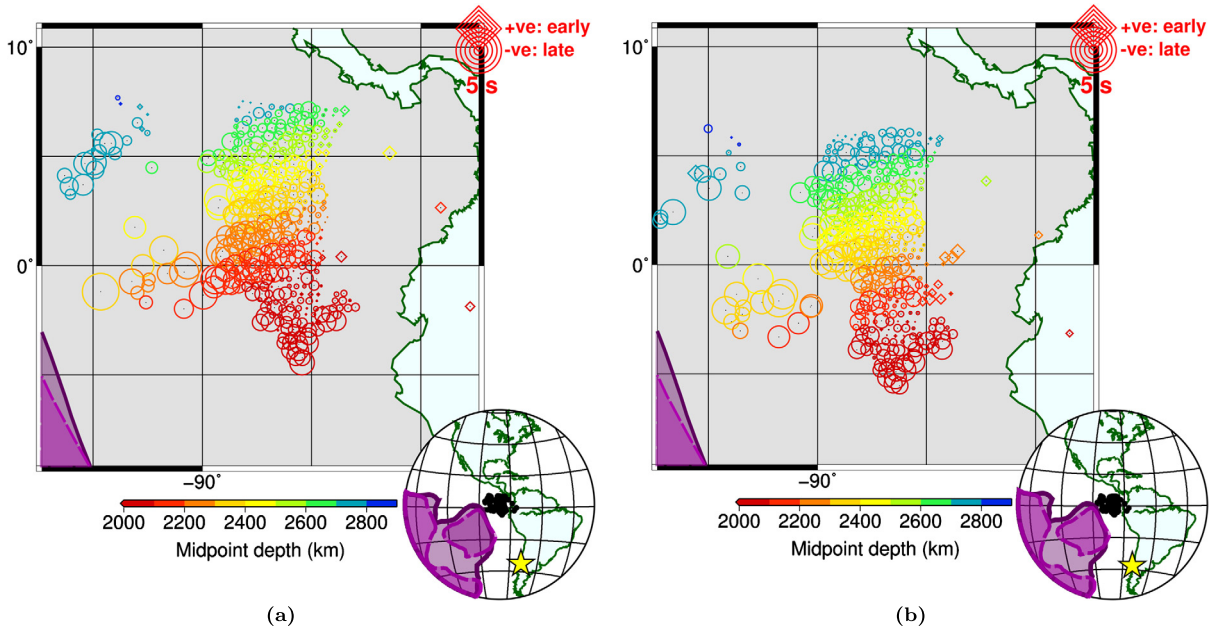

Fig. 3. Residual travel-times shown at turning point location and depth for two events. Diamonds denote early, and circles show late arrivals (by up to 5 s) indicating fast and slow velocities in the lower mantle, respectively. Events occurring on (a) 28/02/2010 at 34.97°S, 71.69°W at 46.5 ± 4.5 km depth, and (b) on 23/04/2010 at 37.54°S, 72.92°W at 43.1 ± 18.3 km depth. The two events are closely located and sample the same region of the lower mantle. LLSVP contours from GyPSuM are shown as purple lines, as defined in Fig. 1. No source-side crustal correction is applied as both events occur below the crust. Inset shows source location as a yellow star, and ray turning points as black circles. Very similar residual patterns are seen for both events suggesting that the signals observed are not dependent on the processing and are independent of the source location.

3. Results

We find laterally varying residual travel-times at all depths with some of the largest deviations detected in the lowermost 300 km of the mantle. We observe patterns of the residual times that are consistent between different source-receiver combinations sampling comparable regions of the lowermost mantle (Fig. 3), showing that our method is robust and the delay times are the result of the mantle structure and not artefacts of our processing. The segments of the LLSVP boundary resolved by individual events show very good agreement and excellent continuity between events, allowing the construction of a continuous boundary (Figs. 4–6, and Supplementary Fig. 2a). The boundary is complex with small scale variations. The resolved P-wave LLSVP boundary is consistent with

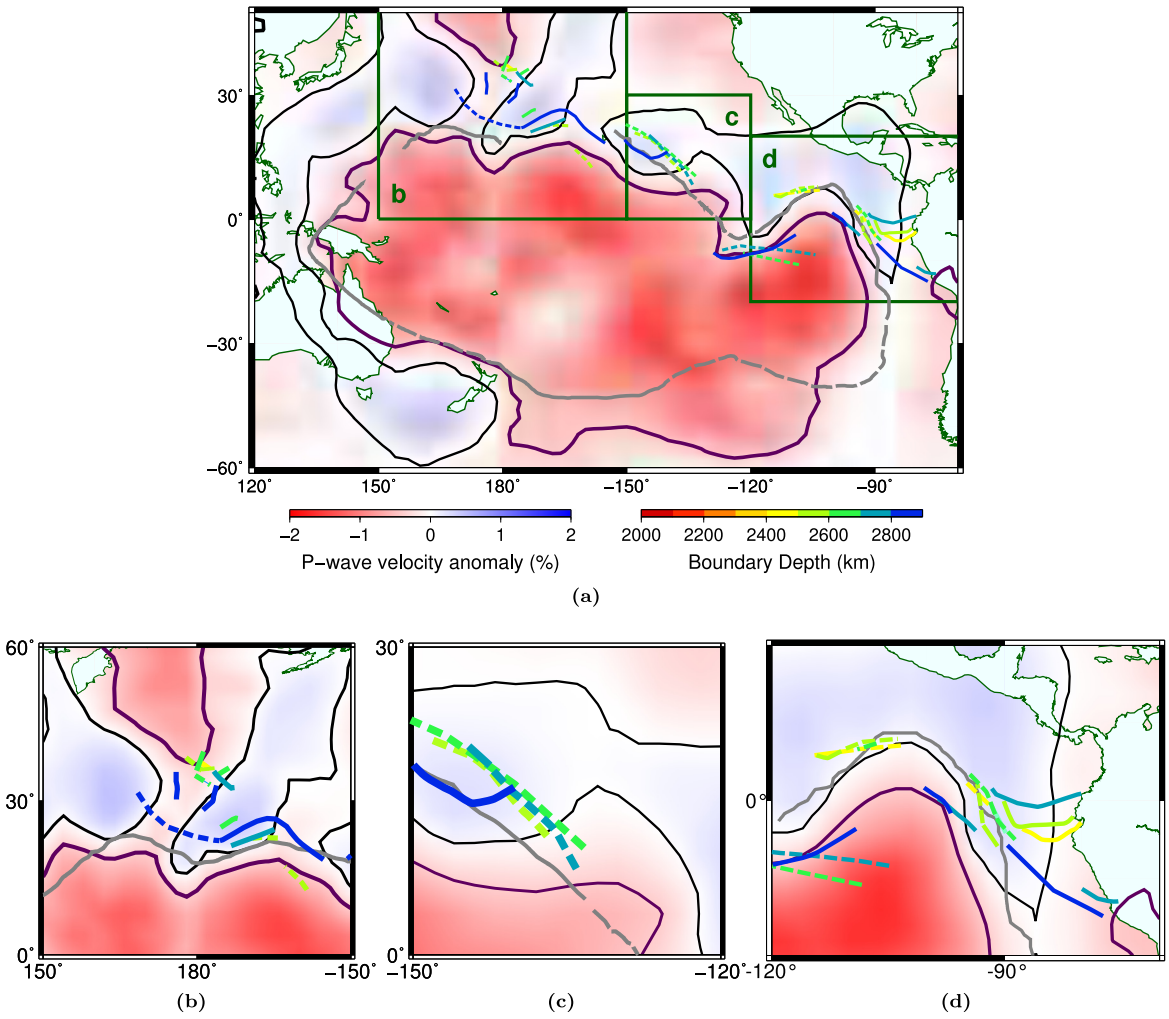

Fig. 4. Location of the P-wave LLSVP boundary determined using the transition from positive to negative travel-time residuals, overlaid on tomography for the lowermost mantle from 2650 km to the CMB (left colour scale) from GyPSuM (Simmons et al., 2010). (a) LLSVP boundary at various heights (right colour scale). Solid lines show the observed transition and dashed lines indicate where a trend towards the boundary (increasing or decreasing residual times) is observed but the actual transition (as a clear zero residual time) is not seen. The boundary of the Pacific LLSVP determined with S-wave travel-times residuals is shown (grey line) (He and Wen, 2012), along with the −0.4% and 0.0% V_P contours in GyPSuM (purple and black lines, respectively) (Simmons et al., 2010). Three subregions of the travel-time boundary, marked by dark green lines, are shown in greater detail: (b) north-west, (c) north-east, and (d) east. Some contours from the tomography models have been removed for figure clarity.

the shape of the boundary as defined in both P-wave tomography model GyPSuM and the S-wave model S40RTS. The boundary can also be defined well above the CMB although this is dependent on ray coverage, i.e. epicentral distance for individual earthquakes.

We use two methods to define the P-wave LLSVP boundary: (1) the area of transition between positive and negative travel-time residuals (the "travel-time residual method"), (2) the largest magnitude of the gradient of the travel-time residuals ("the gradient method") (for examples of both methods see Supplementary Fig. 3). Often the boundary appears to be very sharp, with the transition occurring between two turning points, over as little as 40 km at the eastern edge of the LLSVP (Figs. 7a, 7c, 7e, and 7g). This is consistent with the results from S-wave studies for the African LLSVP which shows similar sharpness (Ni et al., 2002). However, the assumption of a sharp boundary may be inappropriate in some locations; for example, the northern edge of the LLSVP where the boundary appears to be more diffuse (Figs. 7b, 7d, 7f, and 7h). The regions of dominantly positive residuals and dominantly negative residuals appear to be separated by as much as ∼2° (120 km) of small, mixed positive and negative residual travel-times. This transitional region is broader at the CMB and narrows upwards. To the north of the transitional boundary we detect a rapid change in residual time to positive residuals, which appears almost linear (dashed line in Figs. 7d, 7f, 7h) while south of the transitional region the change to negative residuals is more gradual and complex in shape. Although we do not assess the waveforms further in this paper, we note that there is evidence for wavelet broadening along the northern edge of the LLSVP which is not observed for events sampling the eastern edge. However, this could be due to a smaller range of azimuths available for the eastern side. Nonetheless, the boundary is clearly evident in the travel-time residuals. Alternatively, this region of mixed positive and negative travel-time residuals could be the result of the ray geometry relative to the edge of the LLSVP causing rays to travel through both slower and faster material away from the turning point of the ray. On the eastern side of the LLSVP rays are more likely to travel either outside or inside the LLSVP, but due to the small Fresnel zone of the data are unlikely to travel through both, and so do not show a broad variable region.

Using residual travel-times determined at different heights, we trace the boundary of the LLSVP from the CMB up to ∼500 km above the CMB (up to ∼700 km in some regions) (Figs. 4 and 5). We observe variations in the steepness of the detected boundary between the east, and the north–west and north–east sides of the LLSVP, the regions best resolved by our data. Using cross sections through the travel-time residuals at the turning points,

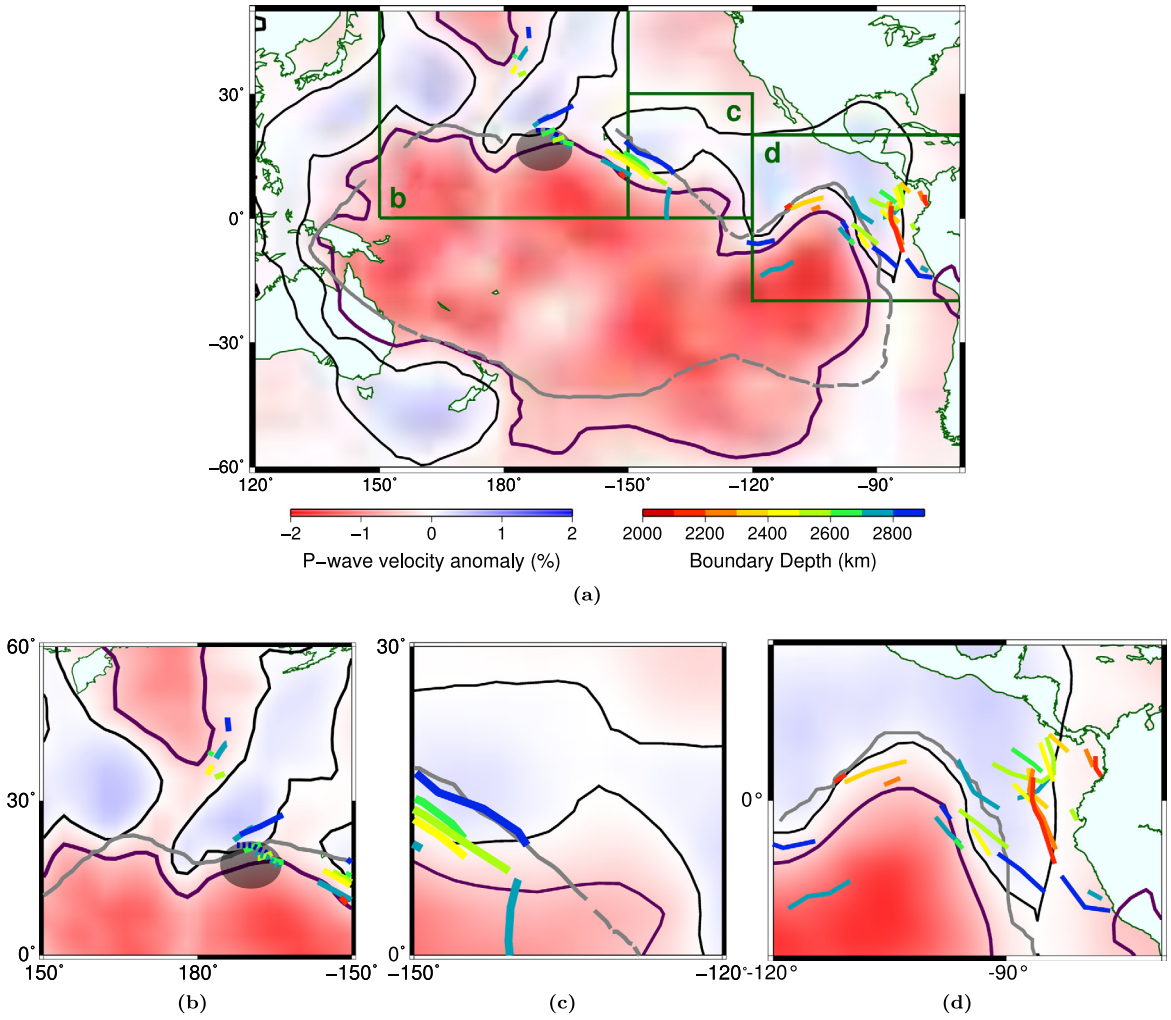

Fig. 5. As Fig. 4 but for the boundary detected using the magnitude of the gradient of travel-time residuals in well-sampled areas. (a) LLSVP boundary at various heights (right colour scale). Solid lines show where the boundary is observed, dotted lines and the grey ellipse show the region of a suspected ULVZ characterised by large magnitude gradients of the travel-time residuals within slow regions. The boundary of the Pacific LLSVP determined with S-waves travel-times residuals is shown (grey line) (He and Wen, 2012), along with the −0.4% and 0.0% V_P contours in GyPSuM (purple and black lines, respectively) (Simmons et al., 2010). Three subregions of the gradient boundary, marked by dark green lines, are shown in greater detail: (b) north–west, (c) north–east, and (d) east. Some contours from the tomography models have been removed for figure clarity.

we visually define the boundary and estimate the slope. We find that the eastern edge is steep at ∼70° (relative to the horizontal) dipping roughly to the north-east, while the northern edge is shallower at ∼26°, dipping north–west (Figs. 7c and 7d).

By calculating the magnitude of the gradient of the travel-time residuals we are better able to observe structure within regions of predominantly positive or negative residual travel-times. Hence, at the northern edge of the LLSVP at ∼20°N, ∼164°W (dotted line in Figs. 5a and 5b, and the southern-most points highlighted in green in Fig. 7b) we observe strong increases of the magnitude of the gradient around large negative travel-time residuals within the lower 200 km of the mantle, consistently observed in all events sampling this region. The localised, sharply defined region shows travel-time residuals of up to −6 s at the CMB, among the highest detected in this study, relative to the corrected model, and is approximately 5° wide. This section of high gradients of the travel-time residuals is contained within a generally slow region and is distinct from the diffuse boundary between positive and negative regions (grey band in Fig. 7b). Due to the large travel-time anomaly, small lateral and vertical extent, and sharp boundary we interpret this area as an ULVZ.

4. Sources of errors

The boundaries of the LLSVP inferred from the P-wave data are very consistent and stable between events (Fig. 3) and the crustal and mantle corrections for 3-D velocity heterogeneity correct for most structure along the path above our region of interest. Nonetheless, there are several potential sources of error that might affect the location of the detected boundary of the LLSVP.

Due to the source-receiver distribution we do not have crossing paths for the LLSVP boundary regions in the lowermost mantle. The lack of crossing paths might cause smearing of the travel-time anomaly along the ray path and rays may encounter lower mantle velocity heterogeneity outside the LLSVP which is then mapped to the ray turning point (e.g. Fig. 2). Additional smearing may be caused by assuming that the turning point represents the main source of the travel-time anomalies, while the travel-time anomaly is accumulated along the path through the lowermost mantle. This could account for the northern edge of the LLSVP being traced ∼10° further north than the −0.4% contour in the tomography model (Fig. 4). The rays in this region will travel through material both slower and faster than PREM, inside and outside of the LLSVP, likely masking the precise point of transition by reducing its

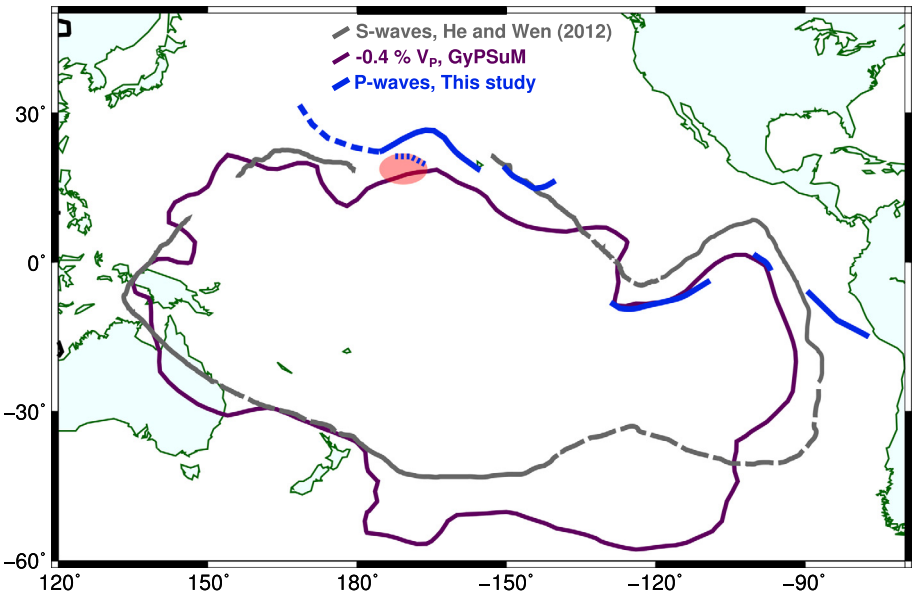

Fig. 6. Best fitting P-wave LLSVP boundary determined using residual travel-time anomalies in the height bin from the CMB to 2800 km depth, as in Fig. 4. The LLSVP boundary determined using S-waves (He and Wen, 2012) and the −0.4% V_P iso-velocity contour from the GyPSuM tomography model (Simmons et al., 2010) are shown as grey and purple lines, respectively. The region of a suspected ULVZ, determined from a large magnitude of the gradient of the travel-time residuals in the height bin from the CMB to 2800 km depth, is shown by the dotted blue line and red ellipse. For coordinates of LLSVP boundary see Supplementary material.

apparent magnitude. This problem also affected S-wave studies of the boundary (He and Wen, 2012), and is a possible cause of the good agreement with this study. Further studies using waveform modelling might give further insight on the location and extent of the velocity anomaly. However, the frequencies used here are currently inappropriate for full 3-D wavefield modelling. We note that the boundaries defined using the magnitude of the gradient of the residuals agree well with those determined by the zero crossing of the travel-time residuals in regions where rays travel parallel to the boundary (the eastern edge of the LLSVP) (Supplementary Fig. 3), but plot further towards the centre of the LLSVP than the zero crossing where the ray travels perpendicular to the boundary (the northern edge of the LLSVP) (Figs. 4 and 5).

We use the REB catalogue because of the high quality source locations (Supplementary Table 1). Lateral location is, on average, defined to within ±10 km of the published hypocentre. Depth, however, is often less well constrained with half of the events used without a published depth and those with depths have average errors of ±7 km. Prior to processing, we choose a depth of 10 km for all events where the depth has not been reported in the catalogue. We test the extent to which these depth variations affect the resulting residual patterns. For hypocentres within the upper crust, depth uncertainties affect the pattern considerably; for example, between a source at the surface and at 10 km depth, for a ray reaching the CMB, there is ∼1 s travel-time difference relative to the 1-dimensional model taking 3-dimensional corrections into account. However, between sources at 10 km and 20 km depth there is only ∼0.03 s travel-time difference. The variation in turning point locations is imperceptible in both circumstances. In summary, source depth uncertainty is only significant for events shallower than 10 km depth.

The applied crustal corrections for the source are static. We believe that this is suitable, given that the difference in the section of the crust sampled by two rays, even with vastly different take-off angles and back-azimuths, is negligible compared to the 1° resolution of the crustal model (Laske et al., 2012). Therefore, inaccuracies in the source depth will affect the delay-time for all stations in the same way, increasing or decreasing all delay-times as a DC shift. The transition from positive to negative residual times will be affected, and so will the point at which the boundary is defined. The amount by which the boundary would move laterally depends on the gradient of the velocity anomalies around the boundary. However, the pattern of residuals relative to each other will not change and so neither will the shape of the boundary. When source depth is poorly constrained or unknown the magnitude of the gradient of the travel-time residuals is a better measure of the location of the LLSVP boundary. However, gradients can only be calculated where there are rays sampling adjacent locations. If sampling of the lower mantle is sparse then gradients cannot be determined. Also, care must be taken not to pick sharp changes in gradient, which result from lack of sampling, as a boundary. This problem can be easily avoided when using travel-time residuals as unsampled regions are apparent and do not distort other travel-time anomalies.

Body-waves are sensitive to off-ray-path structure (Marquering et al., 1998, 1999). However, this is only significant for intermediate and long period waves. Using high-frequency P-waves (∼1 Hz) with the related small Fresnel zone makes this irrelevant and approximation to ray theory allows good predictions of the sampling area. The width of the first Fresnel zone for P-waves sampling the lower mantle with a dominant frequency of 1 Hz is ∼100–140 km (Sato and Fehler, 2008), equivalent to the distance between three stations of the Transportable Array. Therefore, finite-frequency effects may affect the exact location at which the LLSVP boundary is defined, but the location will still be accurate to within 2° orthogonal to the ray path at the turning point of the ray.

The velocity drops observed are likely sufficient to cause diffraction of rays, thus affecting the region of the mantle sampled. However, we use a 2-dimensional ray-tracer which cannot account for this, therefore, it only provides an approximate location of the velocity changes. Using a 3-dimensional ray-tracer could resolve these issues although the tomographic models involved are of low resolution relative to the high-frequency waves used here and would not accurately represent the velocity structure on these scales.

Following crustal and mantle corrections, the remaining residual travel-times represent the deviation of the wave arrival time from that predicted by a 3-D tomography model. Any further errors are due to tomography models not sufficiently explaining

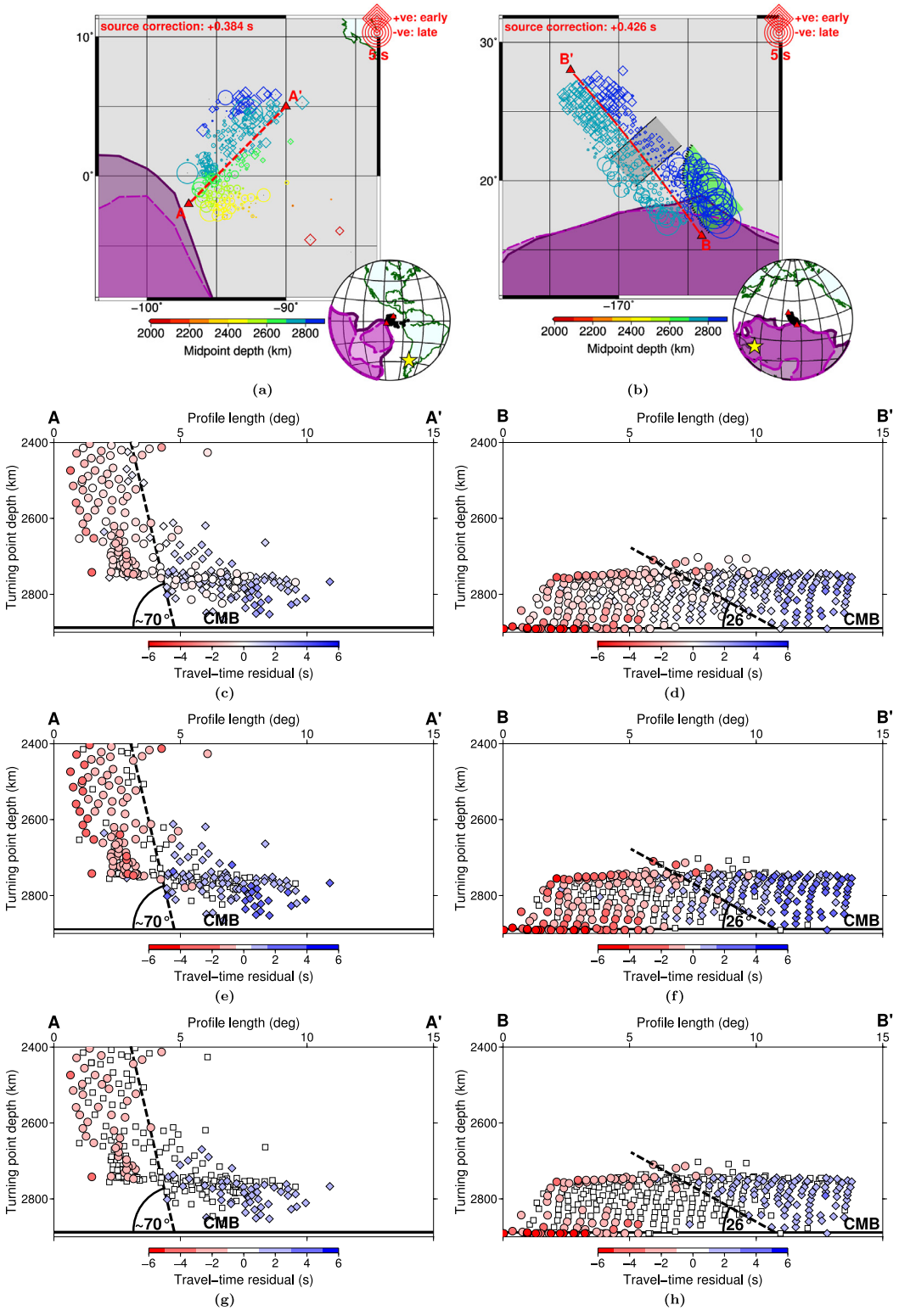

Fig. 7. Residual travel-times shown at turning point location and depth. Diamonds denote early, and circles show late arrivals (by up to 5 s) indicating fast and slow velocities in the lower mantle, respectively. Events occurring on (a) 31/12/2006 at 37.97°S, 71.24°W at 47 ± 17.1 km depth, and on (b) 28/06/2007 at 8.01°S, 154.52°E at 10 km depth. A region of travel-time residuals with varying sign is indicated by grey shading. A region of strong, negative travel-time residuals, interpreted as the location of an ULVZ, separated from the rest of the residuals by a large magnitude gradient of the travel-time residuals, is shown by a dotted line with green shading. The −0.4% V_P iso-velocity contours from GyPSuM at 2500–2650 km and 2650–2900 km (representing the LLSVP boundary) are shown as purple contours and shaded areas, as defined in Fig. 1. Inset shows source (star), ray turning points (circles), and cross-section end points (triangles). Cross-sections through turning points along the red section line shown in the maps for events on (c), (e), (g) 31/12/2006 and (d), (f), (h) on 28/06/2007. The vertical scale is exaggerated by a factor of 2.7. Figures (c) and (d) show travel-time residuals as symbol colour while figures (e), (f), (g), and (h) use more saturated colour scales to highlight the strongest travel-time variations and more clearly mark changes. Dotted lines separating the fast and slow regions are picked by following pronounced changes in magnitude and sign of the travel-time residuals. Travel-time residuals on the eastern edge of the LLSVP show a sharp transition from positive to negative residuals (c), (e), (g), whereas on the northern edge the transition is broader, especially close to the CMB, with a sharp and straight boundary on the northern side of the transition and a complex boundary on the southern side (d), (f), (h). Low travel-time residuals (−0.5 to +0.5 s, and −1 to +1 s, for figures (e) and (f), and (g) and (h), respectively) are shown as white squares.

Earth structure on the scales imaged here and are unavoidable in high frequency studies (Thorne et al., 2013).

5. Discussion

We map out spatially limited but detailed sections of the P-wave boundary between the Pacific LLSVP and the surrounding mantle. We resolve locally complex structure and boundaries of varying steepness. The location of the boundary generally agrees well with that determined using S-waves (He and Wen, 2012) (Fig. 6), not showing any decorrelation of the structure for the different wave types, except for the easternmost extent of the boundary. Local variations of the P-wave and S-wave boundaries do not allow the different resolution of these two probes to be compared.

In the north–west (Figs. 4b and 5b) the LLSVP boundary slopes shallowly to the north–west. However, ray coverage in this location does not allow the boundary to be traced to depths less than ~2600 km, 300 km above the CMB. At the CMB, the boundary is mapped further north than indicated by the 0.0% or −0.4% V_P contours in the tomography model. The high resolution S-wave study (He and Wen, 2012) does not have coverage of the boundary in this location and so the two studies cannot be compared. On the other hand, the boundary matches the −0.4% V_S iso-velocity contour in the S-wave model S40RTS well (Supplementary Fig. 2). The difficulty of delineating a well defined boundary from the travel-times in this region that is in agreement with tomographic models might stem from the broad band of low residual travel-times, which is possibly due to multipathing effects (Fig. 7d). Alternatively, this may represent a region of material with transitional properties from the LLSVP to ambient mantle. This boundary shows further complexity with a 50 km thick layer of small amplitude positive and negative residual travel-times bounded above and below by negative residuals, within the region defined as the LLSVP (Fig. 7h). While this could be the effect of faster material sampled outside of the LLSVP being smeared along the path it could also be the result of double-crossing of perovskite-post-perovskite transition (Hernlund et al., 2005) from relatively slow perovskite above to faster post-perovskite and back again to perovskite close to the CMB (and possibly ULVZ material) as has been observed in a similar region near the edge of the Pacific LLSVP (Lay et al., 2006). Local vertical complexity on the LLSVP boundary, for example an embayment of faster material into the LLSVP, is another possible cause for this feature. However, we cannot test these possibilities further.

In the north–west, north of the LLSVP (~40°N), a transition is observed from fast material in the south to slower material in the north, consistently observed at a range of depths. This area likely is not sampling the boundary of the main LLSVP but might sample a boundary between subducted material and a smaller low velocity region to the north (Figs. 4b and 5b), in good agreement with the tomography model. Our study is not conclusive about whether the LLSVP and this northern outlier are completely separate as the boundary of the Pacific LLSVP in this region is defined only as a trend towards the zero crossing, the transition to positive anomalies is not observed. The P-wave tomography model shows a narrow channel of low velocities between the LLSVP and the outlier suggesting that it is not entirely separate. However, this is not supported by the S-wave tomography model S40RTS in which the outlier does not appear as a coherent feature, nor does it appear consistently in a comparison of recent tomography models (Lekic et al., 2012). This local decorrelation between the P- and S-wave structure may indicate that this material is compositionally different, or might otherwise indicate different resolution between the tomography models. The northern anomaly may be a smaller or "orphaned" thermo-chemical pile in the process of joining with or separating from the main LLSVP (McNamara et al., 2010; Thorne et al., 2013).

The north-eastern boundary determined here (Figs. 4c and 5c) shows a steeper vertical dip than in the north–west, and the position agrees well with that mapped in the S-wave travel-time study (He and Wen, 2012), and the −0.4% V_S contour in the S-wave model S40RTS (Supplementary Fig. 2). At this location, the boundary determined by the gradient method is mapped ~10° further towards the centre of the LLSVP than the boundary from the travel-time residual method, likely due to ray paths propagating perpendicular to the boundary, thus smearing out the travel-time anomaly.

At the eastern edge of the LLSVP (Figs. 4d and 5d) the boundary becomes steeper and shows a sharp transition from fast to slow material. There is a good agreement between the boundaries determined with both the travel-time residual and gradient methods. At this boundary our study matches well with the S-wave study and also the 0.0 % V_P contour in the GyPSuM tomography model, but our boundary deviates significantly from the −0.4% V_S contour (Supplementary Fig. 2). The boundary in this region is likely the best determined as the ray paths travel parallel to it, hence there will be less contamination from other lower mantle structure, and residual times for rays just grazing the LLSVP will be strongly affected. In this region we are also able to observe the boundary at the greatest height above the CMB (~700 km) at the northern tip of the eastern extension of the LLSVP.

Further east of the LLSVP, close to South and Central America, the boundary begins to deviate more significantly from either the LLSVP as defined by the −0.4% iso-velocity contour, or the boundary determined with S-waves (He and Wen, 2012). Our boundary in this region trends east–west along the equator, contrary to other models. Given the consistency of the results from both the travel-time residual and gradient methods in this location (Figs. 4d and 5d), it appears that the boundary is well defined. Given the deviation in shape and location from the rest of the LLSVP and as the boundary close to South America can be traced to ~900 km above the CMB (higher than the LLSVP boundary at ~120°W) (Fig. 5d), we conclude that this is likely not the eastern edge of the Pacific LLSVP but the transition to some other velocity structure and might be related to subduction in this region (Garnero and Lay, 2003; Thomas et al., 2004; Hutko et al., 2006; Thorne et al., 2007; Hutko et al., 2009).

Previously, some studies have reported the LLSVPs to show little to no P-wave velocity change in the lower mantle (Masters et al., 2000; Helmberger and Ni, 2005; Helmberger et al., 2005) while S-wave velocities change significantly. However, we find substantial P-wave velocity variations: waves with travel-time residuals commonly of 4 s relative to PREM (both slower and faster) but up to −6 s, with the travel-time perturbation being attributable to the lowermost 1300 km of the mantle. In a simple 1-D calculation of P-wave velocity anomaly, we assume that the Pacific LLSVP is constrained to the lower 500 or 700 km of the mantle (based both on observations by previous studies (He and Wen, 2012) and the overall maximum and local maximum boundary heights in our study, respectively) and that only part of the ray-path is contained in the LLSVP (as the turning points are often on the edge of the LLSVP) and has a constant velocity reduction with depth, in order to fit the observed −4 s travel-time residual. This can be matched with a 700 km thick layer with ΔV_P of −1.5 to −2.5%, relative to PREM, and a ray travelling through this reduced velocity model for 70 to 50% of its total length. Alternatively, a 500 km thick layer would have to have ΔV_P of −2.2 to −2.9%, relative to PREM. However, we accept that this is a grossly simplified calculation and constraining the wavespeed deviation and velocity structure with waveform modelling would be preferable. Waveform modelling could also be compared to examples of wavelet broadening to determine how

sharp or diffuse the boundaries are. This consideration notwithstanding, these values are similar to those observed in past studies using P_{diff} passing through the African LLSVP (Wen, 2001; Wen et al., 2001).

The relationship between the P- and S-wave boundaries can help determine the material properties. The ratio of S- to P-wave velocity variations ($R_{S,P} = \frac{\delta \ln V_S}{\delta \ln V_P}$) is often used as a measure of the degree to which temperature controls the seismic velocities (Robertson and Woodhouse, 1996a, 1996b). A ratio of <2.5 implies that mantle velocity anomalies are dominated by thermal contributions (Karato, 2003), while ratios larger than this imply that chemical variations are also important. Results of comparing tomography models indicate that the seismic velocity of the mantle is dominantly controlled by chemical variations (Robertson and Woodhouse, 1996a, 1996b; Trampert et al., 2004; Della Mora et al., 2011). However, the validity of this method has been disputed (Schuberth et al., 2009; Davies et al., 2012). Nonetheless, comparing our 1-D velocity calculations with $\Delta V_S \sim -5\%$ calculated for the Pacific LLSVP (He and Wen, 2012) translates to an $R_{S,P}$ of 1.7 to 3.4. The median value of $\sim$2.4 is higher than other high-frequency lower mantle studies (Wysession et al., 1999; Sun et al., 2007), but agrees with large-scale studies (Robertson and Woodhouse, 1996b; Mosca et al., 2012). Using this estimate indicates that the Pacific LLSVP, at least in this region, can be explained by a combination of chemical and thermal anomalies (Karato, 2003). It should be said that this is a maximum estimate for the magnitude of ΔV_P, hence a minimum value of $R_{S,P}$, and by using either a higher LLSVP height ($>$700 km) or a longer ray path through the anomaly (perhaps all of the lower mantle) would produce a smaller ΔV_P. Additionally, this estimate relies on comparing two different studies and using the maximum ΔV_S reported. Using the S-wave information from our dataset processed in a similar way would allow more accurate constraints on the $R_{S,P}$ value of the LLSVP.

Superimposed on the large-scale patterns in residual travel-times, we observe more rapid aberrations in seismic velocities on smaller scales. We see significantly slower seismic velocities in an area previously identified as containing an ULVZ (Luo et al., 2001; Cottaar and Romanowicz, 2012). This region is prominent due to the large magnitude gradient of the travel-time residuals between it and the surrounding slow velocities (Figs. 5b and 7b). The strong gradient is in agreement with other core diffracted wave results (Rost and Garnero, 2006). A simple 1-D calculation through a velocity model with two reduced velocity layers is used to determine the ΔV_P of the ULVZ while the LLSVP is assigned a ΔV_P of -2.7%, calculated above. Residual travel-times increase from -3 s for a P-wave travelling 97° to -6 s for a P_{diff} travelling 99° (Fig. 7d). To account for this additional -3 s residual in the lowermost 35 km of the mantle (the thickness of the mantle that is unique to the second, deeper travelling wave) a velocity reduction of 15–25% is required, very close to that of other ULVZ studies which often report values of $\Delta V_P = -15\%$ using lower frequency $SP_{diff}KS$ (Jensen et al., 2013; Thorne et al., 2013) and using P_{diff} of a similar frequency to this study (Xu and Koper, 2009). However, this calculation has the same limitation as the single layer model of under- or over-estimating the path length within the ULVZ due to not knowing the full lateral extent of the structure. The location of this ULVZ supports the hypothesis that ULVZs can often be found at the edges of, or just within, the LLSVPs (McNamara et al., 2010).

In addition to low velocities (as indicated by negative residuals) we find consistent areas of faster velocities (positive residuals) restricted to the lowermost mantle along the coast of Mexico and South America. This agrees well with many previous studies (Garnero and Lay, 2003; Thomas et al., 2004; Hutko et al., 2006; Thorne et al., 2007; Hutko et al., 2009) showing faster velocities related to subduction of the Farallon slab. As subduction is a top down process it may explain why we see the transition between slow and fast residuals at greater heights in this region than anywhere else in our study (Fig. 5d).

Knowledge of the sharpness of the transition will help to resolve arguments about the degree to which lower mantle anomalies are chemical, thermal, or thermo-chemical in nature (Trampert et al., 2004; Davies et al., 2012). The shape of the LLSVP and the steepness of the walls give constraints on the viscosity and convective support of these features (Tan and Gurnis, 2005; McNamara and Zhong, 2005; Tan and Gurnis, 2007). Previous S-wave studies have used waveform modelling to comment on the dip of the boundary (He and Wen, 2009, 2012). They show the Pacific LLSVP to have both steep and shallow sides on the east and north, respectively, but do not quantify the dip. They demonstrate that the western and eastern boundaries are steeper than those reported for the African LLSVP, and the northern boundary of the Pacific LLSVP is reported as shallowly dipping close to the CMB and steeper at greater heights above the CMB. The African LLSVP is shown to also have laterally varying boundary steepness (Ni and Helmberger, 2003). The northern edge of the African LLSVP is reported to be steeply overturned (Ni et al., 2002), although other studies show that, despite the boundaries being steep, dipping at between 28° and 70°, they are not overturned (Wen, 2001; Wen et al., 2001; Wang and Wen, 2004, 2007; Helmberger et al., 2009). In our study we too find boundaries dipping as steeply as that of the African LLSVP and also with lateral variation in the steepness (Fig. 7). The eastern edge of the Pacific LLSVP shows an apparent dip of $\sim$70°, roughly to the north–east, whereas the northern edge is shallower, dipping at $\sim$26° towards the north–west. Dynamic models of meta-stable, buoyant plumes attempting to take-off from the CMB (Tan and Gurnis, 2005) or a dense, passive body constrained by subduction (McNamara and Zhong, 2005) can both replicate the narrow, curving, and steep-sided nature of the African LLSVP. The Pacific LLSVP's rounder, more dome-like shape, as seen in tomography models, can be generated either by different material properties, relative to the African LLSVP (Tan and Gurnis, 2007), or greater subduction control (McNamara and Zhong, 2005). Using our technique we can track the LLSVP and the associated boundary up to $\sim$700 km above the CMB, matching the heights observed with S-waves (He and Wen, 2012). However, our data coverage does not allow us to mark out the top of the anomaly and so the complete shape cannot be defined.

The boundaries selected in the cross-sections to determine the dip of the flanks of the LLSVP are drawn as straight lines for simplicity and in acknowledgement of the limited constraints. However, a complex, non-linear boundary may be necessary to separate all points. The profiles include points up to 5° either side of the section line hence 3-dimensional structure on the boundary may account for some faster points plotting on slow side of the boundary, and vice versa, when viewed in a 2-dimensional cross section through the middle of the group of points. The boundary selected is also dependent on the angle at which the cross section is determined across the data points, hence the values stated are apparent dips. The location of the boundary and the resulting steepness of the LLSVP should, therefore, be considered an approximation. Nonetheless, the differences observed between the northern and eastern boundaries of the LLSVP are striking and likely to be significant.

Dynamic models imply that active subduction zones can interact with LLSVPs, forcing the less viscous thermo-chemical pile laterally, defining location and shape (McNamara and Zhong, 2005). Therefore, actively subducting slabs may steepen the LLSVP boundary compared to regions where there is no active or recent subduction. We observe that the transition from positive to negative residual times is sharper on the eastern side of the LLSVP than on the northern side (Fig. 7), possibly owing to the closer proximity

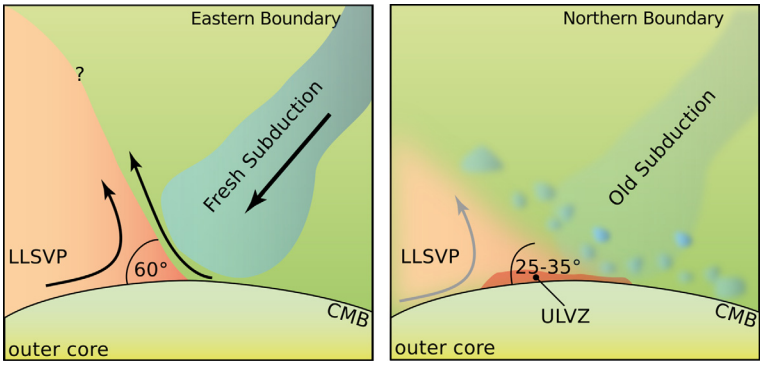

Fig. 8. Conceptual relationship between LLSVP structure and subduction processes. (a) The observed steep (70° dip), sharp (∼40 km) LLSVP boundary in the east may be caused by recently subducted slab material increasing the thermal gradient and shaping the LLSVP. (b) The shallower (26°) and more diffuse (∼120 km) northern boundary, by contrast, may be due to the absence of recent subduction.

to an active subduction zone on the eastern side. The observation of a steeper eastern edge than northern edge agrees with previous S-wave studies (He and Wen, 2012), indicating that this is a robust observation.

We propose that the boundary sharpness and steepness are related to mantle dynamics (Fig. 8). In the eastern Pacific, where there are active subduction zones, the boundary is seismically sharp, occurring over 40 km or less, although resolution is limited by the size of the Fresnel zone. In contrast, the northern edge of the Pacific LLSVP is further from an active subduction zone and has a broader seismic boundary. Subducted material that has been present in the lower mantle for longer will have had longer to thermally, and possibly chemically, equilibrate with ambient conditions through conduction and mechanical mixing, respectively. This would lead to a lower gradient (both thermal and compositional) across the boundary which may present as a lower seismic velocity gradient, hence a wider boundary. Conversely, regions of active subduction where crust and lithosphere has recently been subducted, such as the eastern edge of the Pacific LLSVP, would have higher thermal gradients and, therefore, higher seismic travel-time residual gradients, hence a sharper boundary.

6. Conclusion

We use P-wave travel-time residuals relative to a tomography model to map out the northern and eastern edges of the Pacific LLSVP from the CMB to 700 km above, and other lower mantle structures up to 900 km above the CMB. The northern and eastern regions show contrasting structures: the northern boundary has a seismically broad transition with a shallow slope (∼120 km wide and a dip of ∼26° relative to the horizontal), while the eastern boundary is sharper with a steep slope (∼40 km wide and dipping at 70°). We attribute this to the proximity of the eastern edge to active subduction, steepening and sharpening the boundary through viscous forcing and an increased thermal and/or compositional gradient. Calculation of $R_{S,P}$ to explore the thermal or compositional origin of the LLSVP is complicated by limited data and the result is inconclusive. Contrary to patterns observed in P-wave and bulk-sound tomography models, the P-wave boundary closely matches that determined with S-wave travel times and the 0.0% V_P and −0.4% V_S iso-velocity contours in the GyPSuM and S40RTS models, respectively.

Acknowledgements

We would like to thank the two anonymous reviewers for their productive feedback. D.A.F. is funded by NERC DTG NE/I518750/1. Figures were produced using GMT (Wessel and Smith, 1991) and data was collected from IRIS.

Appendix A. Supplementary material

Supplementary material related to this article can be found online at http://dx.doi.org/10.1016/j.epsl.2014.06.046.

References

Becker, T.W., Kellogg, J.B., Connell, R.J.O., 1999. Thermal constraints on the survival of primitive blobs in the lower mantle. Earth Planet. Sci. Lett. 171, 351–365.

Boyet, M., Carlson, R.W., 2005. 142Nd evidence for early (>4.53 Ga) global differentiation of the silicate Earth. Science, (ISSN 1095-9203) 309 (5734), 576–581. http://dx.doi.org/10.1126/science.1113634. http://www.ncbi.nlm.nih.gov/pubmed/15961629.

Brandenburg, J.P., van Keken, P.E., 2007. Deep storage of oceanic crust in a vigorously convecting mantle. J. Geophys. Res., (ISSN 0148-0227) 112 (B6), B06403. http://dx.doi.org/10.1029/2006JB004813. http://doi.wiley.com/10.1029/2006JB004813.

Burke, K., Steinberger, B., Torsvik, T.H., Smethurst, M.A., 2008. Plume generation zones at the margins of large low shear velocity provinces on the core–mantle boundary. Earth Planet. Sci. Lett., (ISSN 0012-821X) 265 (1–2), 49–60. http://dx.doi.org/10.1016/j.epsl.2007.09.042. http://linkinghub.elsevier.com/retrieve/pii/S0012821X07006036.

Carlson, R., Boyet, M., 2006. Long-term consequences of early Earth differentiation. Geochim. Cosmochim. Acta, (ISSN 0016-7037) 70 (18), A84. http://dx.doi.org/10.1016/j.gca.2006.06.080. http://linkinghub.elsevier.com/retrieve/pii/S0016703706003590.

Castillo, P., 1988. The Dupal anomaly as a trace of the upwelling lower mantle. Nature 336, 667–670.

Christensen, U.R., Hofmann, A.W., 1994. Segregation of subducted oceanic crust in the convecting mantle. J. Geophys. Res. 99, 19844–19867.

Cottaar, S., Romanowicz, B., 2012. An unsually large ULVZ at the base of the mantle near Hawaii. Earth Planet. Sci. Lett., (ISSN 0012-821X) 355–356, 213–222. http://dx.doi.org/10.1016/j.epsl.2012.09.005. http://linkinghub.elsevier.com/retrieve/pii/S0012821X12005006.

Davies, C.J., Gubbins, D., Willis, A.P., Jimack, P.K., 2008. Time-averaged paleomagnetic field and secular variation: Predictions from dynamo solutions based on lower mantle seismic tomography. Phys. Earth Planet. Inter. 169, 194–203. http://dx.doi.org/10.1016/j.pepi.2008.07.021.

Davies, D.R., Goes, S., Davies, J.H., Schuberth, B.S.A., Bunge, H., Ritsema, J., 2012. Reconciling dynamic and seismic models of Earth's lower mantle: the dominant role of thermal heterogeneity. Earth Planet. Sci. Lett., (ISSN 0012-821X) 353–354, 253–269. http://dx.doi.org/10.1016/j.epsl.2012.08.016.

Della Mora, S., Boschi, L., Tackley, P.J., Nakagawa, T., Giardini, D., 2011. Low seismic resolution cannot explain S/P decorrelation in the lower mantle. Geophys. Res. Lett., (ISSN 0094-8276) 38, L12303. http://dx.doi.org/10.1029/2011GL047559. http://doi.wiley.com/10.1029/2011GL047559.

DeMets, C., Gordon, R.G., Argus, D.F., Stein, S., 1990. Current plate motions. Geophys. J. Int. 101, 425–478.

Deschamps, F., Cobden, L., Tackley, P.J., 2012. The primitive nature of large low shear-wave velocity provinces. Earth Planet. Sci. Lett., (ISSN 0012-821X) 349–350, 198–208. http://dx.doi.org/10.1016/j.epsl.2012.07.012. http://linkinghub.elsevier.com/retrieve/pii/S0012821X12003718.

Dupre, B., Allegre, C.J., 1983. Pb–Sr isotope variation in Indian Ocean basalts and mixing phenomena. Nature 303, 142–146.

Dziewonski, A.M., 1984. Mapping the Lower Mantle: determination of lateral heterogeneity in P velocity up to degree and order 6. J. Geophys. Res. 89, 5929–5952.

Dziewonski, A.M., Anderson, D.L., 1981. Preliminary reference Earth model. Phys. Earth Planet. Inter., (ISSN 0031-9201) 25 (4), 297–356. http://dx.doi.org/10.1016/0031-9201(81)90046-7. http://linkinghub.elsevier.com/retrieve/pii/0031920181900467.

Ford, S.R., Garnero, E.J., McNamara, A.K., 2006. A strong lateral shear velocity gradient and anisotropy heterogeneity in the lowermost mantle beneath the southern Pacific. J. Geophys. Res., (ISSN 0148-0227) 111 (B3), 1–14. http://dx.doi.org/10.1029/2004JB003574. http://www.agu.org/pubs/crossref/2006/2004JB003574.shtml.

Frost, D.A., Rost, S., Selby, N.D., Stuart, G.W., 2013. Detection of a tall ridge at the core-mantle boundary from scattered PKP energy. Geophys. J. Int., (ISSN 0956-540X) 195 (1), 558–574. http://dx.doi.org/10.1093/gji/ggt242. http://gji.oxfordjournals.org/cgi/doi/10.1093/gji/ggt242.

Garnero, E.J., Helmberger, D.V., 1995. A very slow basal layer underlying large-scale low-velocity anomalies in the lower mantle beneath the Pacific: evidence from core phases. Phys. Earth Planet. Inter. 9201, 161–176.

Garnero, E.J., Lay, T., 2003. D" shear velocity heterogeneity, anisotropy and discontinuity structure beneath the Caribbean and Central America. Phys. Earth Planet. Inter., (ISSN 0031-9201) 140 (1–3), 219–242. http://dx.doi.org/10.1016/j.pepi.2003.07.014. http://linkinghub.elsevier.com/retrieve/pii/S0031920103001742.

Garnero, E.J., McNamara, A.K., 2008. Structure and dynamics of Earth's lower mantle. Science, (ISSN 1095-9203) 320, 626–628. http://dx.doi.org/10.1126/science.1148028. http://www.ncbi.nlm.nih.gov/pubmed/18451293.

Gubbins, D., Willis, A.P., Sreenivasan, B., 2007. Correlation of Earth's magnetic field with lower mantle thermal and seismic structure. Phys. Earth Planet. Inter. 162, 256–260. http://dx.doi.org/10.1016/j.pepi.2007.04.014.

Hart, S.R., 1984. A large-scale isotope anomaly in the Southern Hemisphere mantle. Nature 309, 753–757.

He, Y., Wen, L., 2009. Structural features and shear-velocity structure of the "Pacific Anomaly". J. Geophys. Res. 114, 1–17. http://dx.doi.org/10.1029/2008JB005814.

He, Y., Wen, L., 2012. Geographic boundary of the "Pacific Anomaly" and its geometry and transitional structure in the north. J. Geophys. Res., (ISSN 0148-0227) 117 (B9), 1–16. http://dx.doi.org/10.1029/2012JB009436. http://www.agu.org/pubs/crossref/2012/2012JB009436.shtml.

Hedlin, M.A.H., Shearer, P.M., 2000. An analysis of large-scale variations in small-scale mantle heterogeneity using Global Seismographic Network recordings of precursors to PKP. J. Geophys. Res. 105 (B6), 13655–13673.

Helmberger, D.V., Ni, S., 2005. Seismic Modeling Constraints on the South African Super Plume. In: Earth's Deep Mantle: Structure, Composition, and Evolution. American Geophysical Union, pp. 63–81.

Helmberger, D.V., Lay, T., Ni, S., Gurnis, M., Hemley, R.J., 2005. Deep mantle structure and the postperovskite phase transition. Proc. Natl. Acad. Sci. USA 102, 17257–17263.

Helmberger, D.V., Sun, D., Liu, L., Tan, E., Gurnis, M., 2009. Review of large low shear velocity provinces in the lower mantle. Geochim. Cosmochim. Acta 73, 520.

Hernlund, J.W., Thomas, C., Tackley, P.J., 2005. A doubling of the post-perovskite phase boundary and structure of the Earth's lowermost mantle. Nature 434, 882–886. http://dx.doi.org/10.1038/nature03496.1.

Hutko, A.R., Lay, T., Garnero, E.J., Revenaugh, J., 2006. Seismic detection of folded, subducted lithosphere at the core-mantle boundary. Nature, (ISSN 1476-4687) 441, 333–336. http://dx.doi.org/10.1038/nature04757. http://www.ncbi.nlm.nih.gov/pubmed/16710418.

Hutko, A.R., Lay, T., Revenaugh, J., 2009. Localized double-array stacking analysis of PcP: D″ and ULVZ structure beneath the Cocos plate, Mexico, central Pacific, and north Pacific. Phys. Earth Planet. Inter., (ISSN 0031-9201) 173, 60–74. http://dx.doi.org/10.1016/j.pepi.2008.11.003. http://linkinghub.elsevier.com/retrieve/pii/S0031920108003452.

Ishii, M., Tromp, J., 1999. Normal-mode and free-air gravity constraints on lateral variations in velocity and density of Earth's mantle. Science, (ISSN 0036-8075) 285, 1231–1236. http://dx.doi.org/10.1126/science.285.5431.1231. http://www.sciencemag.org/cgi/doi/10.1126/science.285.5431.1231.

Jensen, K.J., Thorne, M.S., Rost, S., 2013. SPdKS analysis of ultra-low velocity zones beneath the western Pacific. Geophys. Res. Lett., (ISSN 0094-8276) 40, 4574–4578. http://dx.doi.org/10.1002/grl.50877. http://doi.wiley.com/10.1002/grl.50877.

Karato, S.I., 2003. The Dynamic Structure of the Deep Earth: An Interdisciplinary Approach. Princeton University Press, Princeton, NJ.

Kennett, B.L.N., Engdahl, E.R., 1991. Traveltimes for global earthquake location and phase identification. Geophys. J. Int. 105, 429–465.

Labrosse, S., Hernlund, J.W., Coltice, N., 2007. A crystallizing dense magma ocean at the base of the Earth's mantle. Nature 450, 4–7. http://dx.doi.org/10.1038/nature06355.

Laske, G., Masters, G., Ma, Z., Pasyanos, M.E., 2012. CRUST1.0: an updated global model of Earth's crust. Geophys. Res. Abstr. 14.

Lay, T., Garnero, E.J., 2011. Deep mantle seismic modeling and imaging. Annu. Rev. Earth Planet. Sci. 39, 91–123. http://dx.doi.org/10.1146/annurev-earth-040610-133354.

Lay, T., Hernlund, J., Garnero, E.J., Thorne, M.S., 2006. A post-perovskite lens and D" heat flux beneath the central Pacific. Science, (ISSN 1095-9203) 314, 1272–1276. http://dx.doi.org/10.1126/science.1133280. http://www.ncbi.nlm.nih.gov/pubmed/17124317.

Lekic, V., Cottaar, S., Dziewonski, A., Romanowicz, B., 2012. Cluster analysis of global lower mantle tomography: A new class of structure and implications for chemical heterogeneity. Earth Planet. Sci. Lett., (ISSN 0012-821X) 357–358, 68–77. http://dx.doi.org/10.1016/j.epsl.2012.09.014. http://linkinghub.elsevier.com/retrieve/pii/S0012821X12005109.

Li, M., McNamara, A.K., 2013. The difficulty for subducted oceanic crust to accumulate at the Earth's core-mantle boundary. J. Geophys. Res. 118, 1807–1816. http://dx.doi.org/10.1002/jgrb.50156.

Luo, S.-N., Ni, S., Helmberger, D.V., 2001. Evidence for a sharp lateral variation of velocity at the core–mantle boundary from multipathed PKPab. Earth Planet. Sci. Lett., (ISSN 0012-821X) 189, 155–164. http://dx.doi.org/10.1016/S0012-821X(01)00364-8. http://linkinghub.elsevier.com/retrieve/pii/S0012821X01003648.

Marquering, H., Nolet, G., Dahlen, F., 1998. Three-dimensional waveform sensitivity kernels. Geophys. J. Int., (ISSN 0956-540X) 132 (3), 521–534. http://dx.doi.org/10.1046/j.1365-246X.1998.00426.x. http://doi.wiley.com/10.1046/j.1365-246X.1998.00426.x.

Marquering, H., Dahlen, F.A., Nolet, G., 1999. Three-dimensional sensitivity kernels for finite-frequency traveltimes: the banana-doughnut paradox. Geophys. J. Int. 137, 805–815.

Masters, G., Laske, G., Bolton, H., Dziewonski, A., 2000. The relative behaviour of shear velocity, bulk sound speed, and compressional velocity in the mantle: implications for chemical and thermal structure. In: Earth's Deep Interior: Mineral Physics and Tomography from the Atomic to the Global Scale. In: Geophys. Monogr., vol. 117. American Geophysical Union, pp. 63–87.

McNamara, A.K., Zhong, S., 2005. Thermochemical structures beneath Africa and the Pacific Ocean. Nature, (ISSN 1476-4687) 437, 1136–1139. http://dx.doi.org/10.1038/nature04066. http://www.ncbi.nlm.nih.gov/pubmed/16237440.

McNamara, A.K., Garnero, E.J., Rost, S., 2010. Tracking deep mantle reservoirs with ultra-low velocity zones. Earth Planet. Sci. Lett., (ISSN 0012-821X) 299, 1–9. http://dx.doi.org/10.1016/j.epsl.2010.07.042. http://linkinghub.elsevier.com/retrieve/pii/S0012821X10004802.

Meltzer, A.S., Rudnick, R., Zeitler, P., Levander, A., Humpheys, G., Karlstrom, K., Ekström, G., Carlson, R., Dixon, T., Gurnis, M., Shearer, P., van der Hilst, R.D., 1999. USArray initiative. GSA Today, 8–10.

Mosca, I., Cobden, L., Deuss, A., Ritsema, J., Trampert, J., 2012. Seismic and mineralogical structures of the lower mantle from probabilistic tomography. J. Geophys. Res., (ISSN 0148-0227) 117 (B6), B06304. http://dx.doi.org/10.1029/2011JB008851. http://doi.wiley.com/10.1029/2011JB008851.

Murakami, M., Hirose, K., Kawamura, K., Sata, N., Ohishi, Y., 2004. Post-perovskite phase transition in MgSiO3. Science, (ISSN 1095-9203) 304, 855–858. http://dx.doi.org/10.1126/science.1095932. http://www.ncbi.nlm.nih.gov/pubmed/15073323.

Ni, S., Helmberger, D.V., 2003. Ridge-like lower mantle structure beneath South Africa. J. Geophys. Res., (ISSN 0148-0227) 108, 1–14. http://dx.doi.org/10.1029/2001JB001545. http://www.agu.org/pubs/crossref/2003/2001JB001545.shtml.

Ni, S., Helmberger, D.V., 2003. Seismological constraints on the South African superplume; could be the oldest distinct structure on earth. Earth Planet. Sci. Lett. 206, 119–131.

Ni, S., Tan, E., Gurnis, M., Helmberger, D., 2002. Sharp sides to the African superplume. Science, (ISSN 1095-9203) 296, 1850–1852. http://dx.doi.org/10.1126/science.1070698. http://www.ncbi.nlm.nih.gov/pubmed/12052955.

Oganov, A.R., Ono, S., 2004. Theoretical and experimental evidence for a post-perovskite phase of MgSiO3 in Earth's D″ layer. Nature 430, 445–448.

Panning, M., Romanowicz, B., 2006. A three-dimensional radially anisotropic model of shear velocity in the whole mantle. Geophys. J. Int., (ISSN 0956-540X) 167 (1), 361–379. http://dx.doi.org/10.1111/j.1365-246X.2006.03100.x. http://gji.oxfordjournals.org/cgi/doi/10.1111/j.1365-246X.2006.03100.x.

Rawlinson, N., Kennett, B.L.N., 2004. Rapid estimation of relative and absolute delay times across a network by adaptive stacking. Geophys. J. Int., (ISSN 0956-540X) 157 (1), 332–340. http://dx.doi.org/10.1111/j.1365-246X.2004.02188.x. http://gji.oxfordjournals.org/cgi/doi/10.1111/j.1365-246X.2004.02188.x.

Richards, M.A., Engebretson, D.C., 1992. Large-scale mantle convection and the history of subduction. Nature 355, 437–440.

Richards, M.A., Ricard, Y., Lithgow-Bertelloni, C., Spada, G., Sabadini, R., 1997. An Explanation for Earth's Long-Term Rotational Stability. Science, (ISSN 0036-8075) 275 (5298), 372–375. http://dx.doi.org/10.1126/science.275.5298.372. http://www.sciencemag.org/cgi/doi/10.1126/science.275.5298.372.

Ritsema, J., Garnero, E.J., Lay, T., 1997. A strongly negative shear velocity gradient and lateral variability in the lowermost mantle beneath the Pacific. J. Geophys. Res. 102, 20395–20411.

Ritsema, J., Ni, S., Helmberger, D.V., Crotwell, H.P., 1998. Evidence for strong shear velocity reductions and velocity gradients in the lower mantle beneath Africa. Geophys. Res. Lett. 25, 4245–4248.

Ritsema, J., van Heijst, H.J., Woodhouse, J.H., 1999. Complex Shear Wave Velocity Structure Imaged Beneath Africa and Iceland. Science, (ISSN 0036-8075) 286 (5446), 1925–1928. http://dx.doi.org/10.1126/science.286.5446.1925. http://www.sciencemag.org/cgi/doi/10.1126/science.286.5446.1925.

Ritsema, J., Deuss, A., van Heijst, H.J., Woodhouse, J.H., 2011. S40RTS: a degree-40 shear-velocity model for the mantle from new Rayleigh wave dispersion, teleseismic traveltime and normal-mode splitting function measurements. Geophys. J. Int., (ISSN 0956-540X) 184 (3), 1223–1236. http://dx.doi.org/10.1111/j.1365-246X.2010.04884.x. http://gji.oxfordjournals.org/cgi/doi/10.1111/j.1365-246X.2010.04884.x.

Robertson, G.S., Woodhouse, J.H., 1996a. Constraints on lower mantle physical properties from seismology and mineral physics. Earth Planet. Sci. Lett. 143, 197–205.

Robertson, G.S., Woodhouse, J.H., 1996b. Ratio of relative S to P velocity heterogeneity in the lower mantle. J. Geophys. Res. 101, 20041–20052.

Rost, S., Garnero, E.J., 2004. A study of the uppermost inner core from PKKP and P'P' differential traveltimes. Geophys. J. Int., (ISSN 0956-540X) 156, 565–574. http://dx.doi.org/10.1111/j.1365-246X.2004.02139.x. http://doi.wiley.com/10.1111/j.1365-246X.2004.02139.x.

Rost, S., Garnero, E.J., 2006. Detection of an ultralow velocity zone at the core-mantle boundary using diffracted PKKP ab waves. J. Geophys. Res., (ISSN 0148-0227) 111, 1–8. http://dx.doi.org/10.1029/2005JB003850. http://www.agu.org/pubs/crossref/2006/2005JB003850.shtml.

Rost, S., Garnero, E.J., Williams, Q., Manga, M., 2005. Seismological constraints on a possible plume root at the core-mantle boundary. Nature, (ISSN 1476-4687) 435, 666–669. http://dx.doi.org/10.1038/nature03620. http://www.ncbi.nlm.nih.gov/pubmed/15931220.

Sato, H., Fehler, M.C., 2008. Seismic Wave Propagation and Scattering in the Heterogeneous Earth, 2nd edn. Springer Verlag, AIP Press, New York.

Schuberth, B.S.A., Bunge, H.-P., Ritsema, J., 2009. Tomographic filtering of high-resolution mantle circulation models: Can seismic heterogeneity be explained by temperature alone? Geochem. Geophys. Geosyst., (ISSN 1525-2027) 10. http://dx.doi.org/10.1029/2009GC002401. http://www.agu.org/pubs/crossref/2009/2009GC002401.shtml.

Simmons, N.A., Forte, A.M., Boschi, L., Grand, S.P., 2010. GyPSuM: A joint tomographic model of mantle density and seismic wave speeds. J. Geophys. Res., (ISSN 0148-0227) 115 (B12), B12310. http://dx.doi.org/10.1029/2010JB007631. http://doi.wiley.com/10.1029/2010JB007631.

Steinberger, B., Torsvik, T.H., 2008. Absolute plate motions and true polar wander in the absence of hotspot tracks. Nature, (ISSN 1476-4687) 452 (7187), 620–623. http://dx.doi.org/10.1038/nature06824. http://www.ncbi.nlm.nih.gov/pubmed/18385737.

Sun, X., Song, X., Zheng, S., Helmberger, D.V., 2007. Evidence for a chemical-thermal structure at base of mantle from sharp lateral P-wave variations beneath Central America. Proc. Natl. Acad. Sci. USA 104, 26–30.

Tan, E., Gurnis, M., 2005. Metastable superplumes and mantle compressibility. Geophys. Res. Lett., (ISSN 0094-8276) 32, 1–4. http://dx.doi.org/10.1029/2005GL024190. http://www.agu.org/pubs/crossref/2005/2005GL024190.shtml.

Tan, E., Gurnis, M., 2007. Compressible thermochemical convection and application to lower mantle structures. J. Geophys. Res., (ISSN 0148-0227) 112 (B6), B06304. http://dx.doi.org/10.1029/2006JB004505. http://doi.wiley.com/10.1029/2006JB004505.

Thomas, C., Garnero, E.J., Lay, T., 2004. High-resolution imaging of lowermost mantle structure under the Cocos plate. J. Geophys. Res., (ISSN 0148-0227) 109, 1–11. http://dx.doi.org/10.1029/2004JB003013. http://www.agu.org/pubs/crossref/2004/2004JB003013.shtml.

Thorne, M., Garnero, E.J., Grand, S.P., 2004. Geographic correlation between hot spots and deep mantle lateral shear-wave velocity gradients. Phys. Earth Planet. Inter., (ISSN 0031-9201) 146, 47–63. http://dx.doi.org/10.1016/j.pepi.2003.09.026. http://linkinghub.elsevier.com/retrieve/pii/S003192010400113X.

Thorne, M.S., Lay, T., Garnero, E.J., Jahnke, G., Igel, H., 2007. Seismic imaging of the laterally varying D″ region beneath the Cocos Plate. Geophys. J. Int., (ISSN 0956-540X) 170, 635–648. http://dx.doi.org/10.1111/j.1365-246X.2006.03279.x. http://doi.wiley.com/10.1111/j.1365-246X.2006.03279.x.

Thorne, M.S., Garnero, E.J., Jahnke, G., Igel, H., McNamara, A.K., 2013. Mega ultra low velocity zone and mantle flow. Earth Planet. Sci. Lett., (ISSN 0012-821X) 364, 59–67. http://dx.doi.org/10.1016/j.epsl.2012.12.034. http://linkinghub.elsevier.com/retrieve/pii/S0012821X12007200.

Thorne, M.S., Zhang, Y., Ritsema, J., 2013. Evaluation of 1-D and 3-D seismic models of the Pacific lower mantle with S, SKS, and SKKS traveltimes and amplitudes. J. Geophys. Res., Solid Earth, (ISSN 2169-9313) 118 (3), 985–995. http://dx.doi.org/10.1002/jgrb.50054. http://doi.wiley.com/10.1002/jgrb.50054.

To, A., Romanowicz, B., Capdeville, Y., Takeuchi, N., 2005. 3D effects of sharp boundaries at the borders of the African and Pacific Superplumes: Observation and modeling. Earth Planet. Sci. Lett., (ISSN 0012-821X) 233, 137–153. http://dx.doi.org/10.1016/j.epsl.2005.01.037. http://linkinghub.elsevier.com/retrieve/pii/S0012821X05001007.

Torsvik, T.H., Smethurst, M.A., Burke, K., Steinberger, B., 2006. Large igneous provinces generated from the margins of the large low-velocity provinces in the deep mantle. Geophys. J. Int., (ISSN 0956-540X) 167, 1447–1460. http://dx.doi.org/10.1111/j.1365-246X.2006.03158.x. http://doi.wiley.com/10.1111/j.1365-246X.2006.03158.x.

Trampert, J., Deschamps, F., Resovsky, J., Yuen, D., 2004. Probabilistic tomography maps chemical heterogeneities throughout the lower mantle. Science, (ISSN 1095-9203) 306, 853–856. http://dx.doi.org/10.1126/science.1101996. http://www.ncbi.nlm.nih.gov/pubmed/15514153.

Trønnes, R.G., 2010. Structure, mineralogy and dynamics of the lowermost mantle. Mineral. Petrol., (ISSN 0930-0708) 99, 243–261. http://dx.doi.org/10.1007/s00710-009-0068-z. http://www.springerlink.com/index/10.1007/s00710-009-0068-z.

van Keken, P.E., Hauri, E.H., Brandenburg, J.P., Ballentine, C.J., 2010. Generation of mantle heterogeneity by ocean crust recycling: Geophysical and geochemical constraints. Geochim. Cosmochim. Acta 74, 1072.

Wang, Y., Wen, L., 2004. Mapping the geometry and geographic distribution of a very low velocity province at the base of the Earth's mantle. J. Geophys. Res., (ISSN 0148-0227) 109 (B10), B10305. http://dx.doi.org/10.1029/2003JB002674. http://www.agu.org/pubs/crossref/2004/2003JB002674.shtml.

Wang, Y., Wen, L., 2007. Geometry and P and S velocity structure of the "African Anomaly". J. Geophys. Res., (ISSN 0148-0227) 112, 1–26. http://dx.doi.org/10.1029/2006JB004483. http://www.agu.org/pubs/crossref/2007/2006JB004483.shtml.

Wen, L., 2001. Seismic evidence for a rapidly varying compositional anomaly at the base of the Earth's mantle beneath the Indian Ocean. Earth Planet. Sci. Lett., (ISSN 0012-821X) 194, 83–95. http://dx.doi.org/10.1016/S0012-821X(01)00550-7. http://linkinghub.elsevier.com/retrieve/pii/S0012821X01005507.

Wen, L., Silver, P., James, D., Kuehnel, R., 2001. Seismic evidence for a thermochemical boundary at the base of the Earth's mantle. Earth Planet. Sci. Lett., (ISSN 0012-821X) 189, 141–153. http://dx.doi.org/10.1016/S0012-821X(01)00365-X. http://linkinghub.elsevier.com/retrieve/pii/S0012821X0100365X.

Wessel, P., Smith, W.H.F., 1991. Free software helps map and display data. EoS Trans. 72, 441–448.

Williams, Q., Revenaugh, J., Garnero, E.J., 1998. A correlation between ultra-low basal velocities in the mantle and hot spots. Science 281, 546–549. http://dx.doi.org/10.1126/science.281.5376.546. http://www.sciencemag.org/cgi/doi/10.1126/science.281.5376.546.

Wysession, M.E., Langenhorst, A., Fouch, M.J., Fischer, K.M., Al-eqabi, G.I., Shore, P.J., Clarke, T.J., 1999. Lateral variations in compressional/shear velocities at the base of the mantle. Science 284, 120–125.

Xu, Y., Koper, K.D., 2009. Detection of a ULVZ at the base of the mantle beneath the northwest Pacific. Geophys. Res. Lett., (ISSN 0094-8276) 36, 1–5. http://dx.doi.org/10.1029/2009GL039387. http://www.agu.org/pubs/crossref/2009/2009GL039387.shtml.